Characteristics of the crystalline and luminescence properties of a-plane GaN films grown on γ-$LiAlO_2$ (302) substrates

Tingting Jia (贾婷婷)[1,2*], Shengming Zhou (周圣明)[1,2], Hui Lin (林 辉)[1,2], Hao Teng (滕 浩)[1,2], Xiaorui Hou (侯肖瑞)[1,2], Jianqi Liu (刘建奇)[2,3], Jun Huang (黄 俊)[2,3], Min Zhang (张 敏)[2,3], Jianfeng Wang (王建峰)[3], and Ke Xu (徐 科)[3]

[1]*Shanghai Institute of Optics and Fine Mechanics, Chinese Academy of Sciences, Shanghai 201800, China*

[2]*Graduate University of Chinese Academy of Sciences, Beijing 100049, China*

[3]*Suzhou Institute of Nano-Tech and Nanobionics, Chinese Academy of Sciences, Suzhou 215123, China*

[*]*Corresponding author: jiating8500@163.com*

Received March 18, 2011; accepted April 21, 2011; posted online July 11, 2011

A-plane GaN films are deposited on (302) γ-$LiAlO_2$ substrates by metalorganic chemical vapor deposition (MOCVD). The X-ray diffraction (XRD) results indicate that the in-plane orientation relationship between GaN and LAO substrates is $[010]_{LAO} /\!/ [0001]_{GaN}$ and $[203]_{LAO} /\!/ [1\bar{1}00]_{GaN}$ with 0.03% and 2.85% lattice mismatch, respectively. Raman scattering results indicate that the strain in the films decreases along with the increase in the thickness of the films. In addition to the band edge emission at 3.42 eV, defects-related luminescence at 3.35 eV is observed in the photoluminescence (PL) spectra. The cathodoluminescence (CL) spectra indicate that the 3.35-eV emission is related to the V pits.

OCIS codes: 310.6860, 310.0310, 310.1860, 300.6470.

doi: 10.3788/COL201109.093101.

Nitride-based light emitting diodes (LEDs) with spectral range from ultraviolet to amber are already commercially available. GaN-based devices such as LEDs, laser diodes (LDs), and high electron mobility transistor (HEMT) were widely invested[1−3]. However, GaN and its compounds suffer from polarization fields when grown along the c-[0001] direction. These polarization fields result in poor carrier recombination efficiencies in quantum wells and shift in emission wavelength caused by the quantum-confined stark effect (QCSE) due to the spatial separation of the electron and the hole wave function separation[4]. Nonpolar nitride materials, namely $\{1\bar{1}00\}$ m-plane or $\{11\bar{2}0\}$ a-plane, have been explored to eliminate the strong internal electric fields in the active regions of optoelectronic devices and improve the efficiency of nitride devices. The γ-$LiAlO_2$ (LAO) substrates attracted considerable attention due to their small lattice misfit for GaN. Most of the nonpolar GaN films based on (100)-plane LAO substrate turned out to be $\{1\bar{1}00\}$ m-plane[5−7]. However, the typical surface of LAO, the (100) plane, exhibits a periodic trench pattern, although with low roughness values[8]. The trench morphology was harmful to the GaN films grown on it. Recently, we found that it was easier to attain a trench-free surface by polishing the (302) plane of the LAO substrate[9]. A-plane ZnO films had been fabricated on the (302) plane of LAO[10].

In this letter, GaN films are deposited on (302)-oriented well-polished LAO substrates by metalorganic chemical vapor deposition (MOCVD). Single $[11\bar{2}0]$ orientation is confirmed by a ω-2θ scan of X-ray diffraction (XRD). The in-plane orientation relationship between GaN and LAO substrates is investigated by high-resolution XRD (HRXRD). The strain in GaN films is measured by Raman scattering. In addition, the luminescence properties of the as-grown films are also characterized.

High-quality LAO crystal was grown by the improved Czochralski technique. All film growth experiments have been performed in an MOCVD system (Aixtron, German). Prior to the growth process, the substrates were sequentially dipped in propane and ethanol with an ultrasonic bath. The GaN deposition process can be separated into four different stages: substrate nitridation, buffer layer deposition, low-temperature GaN deposition, and high-temperature deposition. The growth process was described in detail[11]. The film thickness of GaN was determined by the deposition time. Herein, four samples with thickness of 155, 585, 850, and 1 860 nm (respectively marked as S1, S2, S3, and S4) were discussed, respectively.

The structure and orientation of GaN were studied by XRD. Room temperature photoluminescence (RT-PL) was obtained by using a continuous wave (CW) He–Cd laser (325 nm). Scanning electron microscope (SEM) and cathodoluminescence (CL) were also used to investigate the luminescence properties.

Figure 1(a) shows the ω-2θ scans of the samples. The growth surface of all the samples was determined to be $(11\bar{2}0)$ a-plane, and the (302) plane of the LAO substrate was detected as well. By comparing the intensity of the GaN $(11\bar{2}0)$ reflection for the samples in Fig. 1(a), it is clear that the GaN $(11\bar{2}0)$ reflection tends to become more intense with an increase in film thickness. The full-width at half-maximum (FWHM) values of the ω rocking curves range from 684″ to 1 230″ for the $(11\bar{2}0)$ peak of the samples (Fig. 1(b)). The FWHM values of $(11\bar{2}0)$ were reduced from S1 to S4, indicating that when the film grows thicker, the crystal quality of the GaN film improves faster. For the purpose of confirming

 © 2011 Chinese Optics Letters

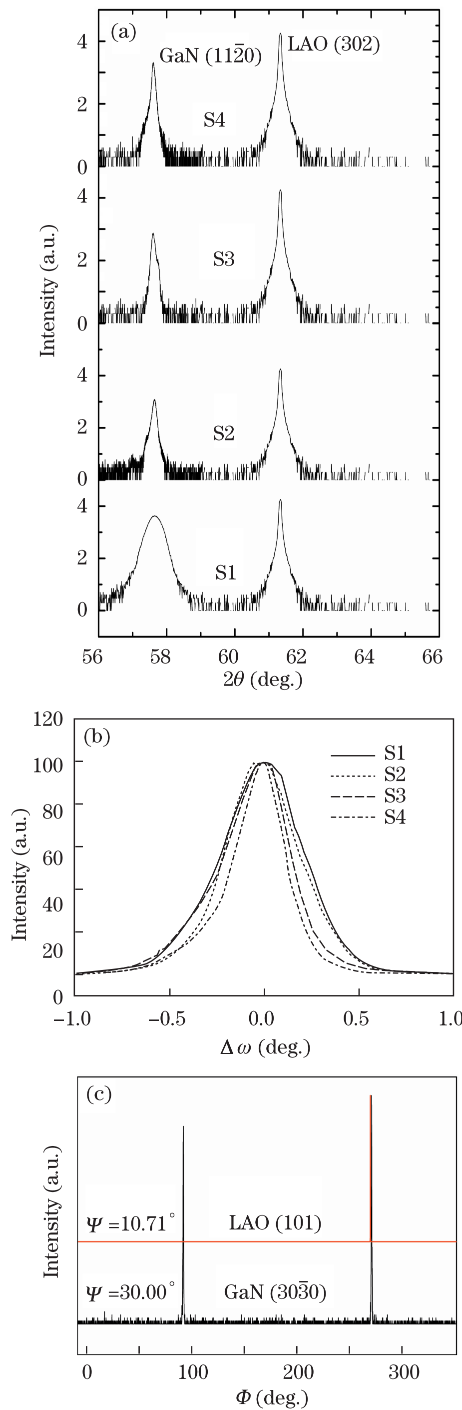

Fig. 1. (a) $\omega - 2\theta$ scans, (b) rocking curves of the GaN films, and (c) off-axis Φ scans were used to determine the relationship between the GaN epitaxy and the LAO substrate.

the in-plane orientation of GaN with respect to the LAO, the off-axis Φ scan in skew-symmetry geometry is applied in this case. Two rotations, ϕ and φ, are adjusted in the scanning. ϕ is the angle of rotation around the normal sample surface, whereas φ is the angle between the surface of the sample and the scattering plane. In practice, after tilting the sample to the correct φ for a particular off-axis reflection, the ϕ scans are used to detect GaN (30$\bar{3}$0), (30$\bar{3}$3), and LAO (300) peaks, as shown in Fig. 1(c). The correlation between the ϕ positions of these peaks determines the following epitaxial relationship: $[1\bar{1}00]_{\mathrm{GaN}}/\!/[\bar{2}03]_{\mathrm{LAO}}$ and $[0001]_{\mathrm{GaN}}/\!/[010]_{\mathrm{LAO}}$. As the lattice parameters are a_{LAO}=0.5169 nm, c_{LAO}=0.6268 nm, a_{GaN}=0.3186 nm, and c_{GaN}=0.5176 nm, the mismatch between the substrate and the film is calculated by $f = (a_{\mathrm{s}} - a_{\mathrm{f}})/a_{\mathrm{f}}$, where f means the mismatch coefficient, a_{s} and a_{f} indicate the lattice parameters of the substrate and the film, respectively. $[010]_{\mathrm{LAO}}/\!/[0001]_{\mathrm{GaN}}$=−0.30%, and $[203]_{\mathrm{LAO}}/\!/[1\bar{1}00]_{\mathrm{GaN}}$=−2.85%.

The Raman scattering was used to characterize the strain in nonpolar GaN films. A serial of GaN films as prepared was put to the test. In this letter, we only consider the first-order phonon Raman scattering with wave vector k–0 (Γ point). In the wurtzite structure GaN, the E_2(H) mode represents the atom vibration perpendicular to the c axis and is greatly affected by the stress induced in the film. The backscattering spectra of the GaN layer with no polarization are displayed in Fig. 2. In the spectra of S1, the A_1(TO) mode was weakly detected; no significant peak of the E_2(H) mode was detected. Since S1 was very thin, the property of the crystalline was low and the vibration of N atoms perpendicular to the c axis was slightly detected. As the films grew thicker, the E_2(H) mode started to be detected and the intensity rose sharply; as to S4, the intensity of the E_2(H) mode became the strongest. However, the intensity of the A_1(TO) mode did not change significantly from S1 to S4. The strain perpendicular to the c axis in GaN films

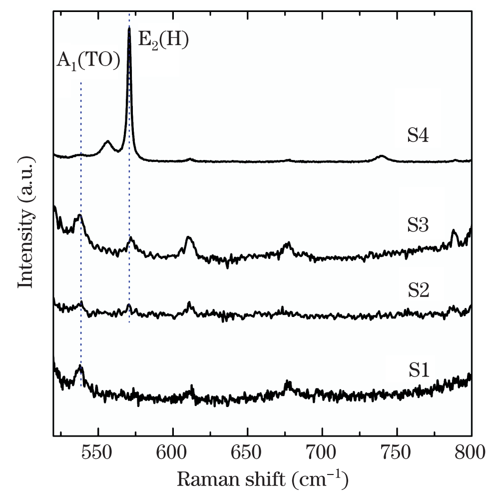

Fig. 2. Raman scattering spectra of the as-grown GaN films.

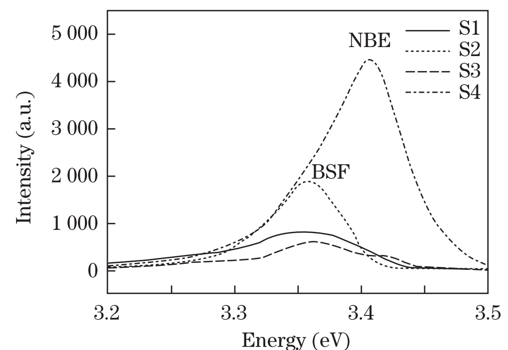

Fig. 3. RT-PL of the as-grown GaN films and two emissions, at 3.42 and 3.35 eV, are observed. NBE: near band edge; BSF: basal plane stacking faults.

Table 1. Parameters of GaN Films on LAO (302) Obtained by Raman Scattering Spectra

	E_2(H) mode		
	Raman Shift (cm^{-1})	$\Delta\omega$ (cm^{-1})	σ (Gpa)
S1	573.53	5.93	1.412
S2	571.78	4.18	0.995
S3	570.54	2.94	0.700
S4	570.52	2.92	0.695

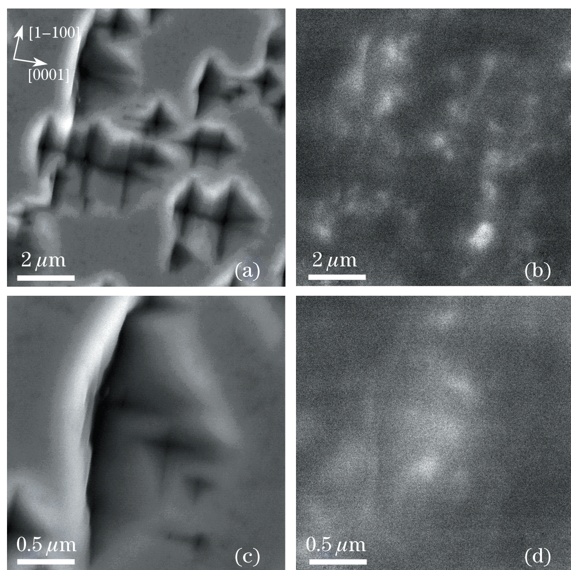

Fig. 4. (a) SEM images and (b) CL panchromatic micrograph for pits on the surface of S3; (c) SEM image of the pits by high magnification and (d) monochromatic CL micrograph at 3.35 eV.

was calculated by the formula $\sigma = \Delta\omega p$, where $\Delta\omega$ is the Raman shift from bulk GaN (567.8 cm^{-1} for E_2(H)[12]) and p is a constant ($p_{GaN} = 4.2$ cm^{-1}/Gpa). The Raman shift and strain of the samples are listed in Table 1. As shown in the table, the Raman shift of E_2(H) became lower as the films grew thicker. This indicates that the strain in the films became lower when the thickness increased. The crystalline quality of GaN was improved when the thickness of the film increased.

The RT-PL spectra of the samples were dominated by the near band edge (NBE) emission at 3.42 eV, as shown in Fig. 3. Emission at 3.35 eV was also observed, and the peak intensity was reduced when the films became thicker. Several groups attributed this transition to structural defects, or rather type I_2 basal plane stacking faults (BSFs)[9]. No NBE band was observed for samples S1 and S2. Both the BSFs and NBE bands were detected for S3. A wide emission band with asymmetric shape was tested for S4, which could comprise the BSFs and NBE bands. Since the film thickness was increased from S1 to S4, it is inferred that the crystallinity improvement by increasing the film thickness promoted the PL luminescence. This indicates that the crystalline quality was improved when the thickness increased. The rather weak emissions at 3.42 and 3.35 eV observed in the spectrum of S3 were consider as "thermal quenching" in the cooling process[13]. Thus, the results reveal that the BSFs can inhibit luminescence from the NBE.

The luminescence properties in S3 were further investigated. There are some pits on the surface of S3 with triangle or square shape, as shown in Fig. 4(a). The pits morphology refers to the in-plane asymmetric growth rates of the N and Ga faces. In addition, the pits are considered as part of three-dimensional hexagonal pyramids lying in the growth plane with the tips pointing to the $[000\bar{1}]$ direction[14]. There were little reports on the square-shaped pits; the origin of these pits might be similar with the triangle ones. An interesting morphology was that two square-shaped pits often appear in pair. Additionally, the diagonal line of these pits is parallel to the [0001] and $[1\bar{1}00]$ directions of GaN, respectively. CL was used to investigate the distribution of defects emission. It was considered that the 3.35-eV emissions associated with type I_2 BSFs were combined to the pits[15]. The type I_2 BSFs were considered as a thin zinc-blende quantum wells embedded in the wurtzite matrix with type II alignment. Figure 4(b) was a panchromatic micrograph of the pits. The monochromatic CL measurement at 3.35 eV was used to investigate the pits in a higher magnitude, as shown in Fig. 4(d). Corresponding to the SEM image of the pit in Fig. 4(c), the spot pattern emission was from the center of the small square pits located at the edge of the big triangle pit, indicating that many holes from the A valence band were involved in the emission. A rough assumption was adopted to interpret the origin of these pits: it was supposed to be a part of zinc-blende pyramids implanted in the wurtzite nonpolar surface. The photo-generated electrons are captured in such structures and recombine with the holes localized in a triangular potential notch formed in the barrier due to the discontinuity of the spontaneous polarization across the interfaces between zinc blend and wurtzite structure, and formed a barrier that restricted many holes in a potential notch. When the photo-generated electrons were captured and recombined with these holes, the emission was observed. Further investigation will be focused on the verification of this assumption.

In conclusion, we figure out the in-plane relationship between a-GaN and LAO (302). The strain in GaN films with different thicknesses is investigated by Raman scattering. It turns out that the quality is improved when the film is grown thicker. In addition, the luminescence properties are investigated. The PL spectra also indicate a strain relaxation when the film thickness is increased. Emissions at 3.35 and 3.42 eV are concerned with the defects in the films and the NBE emission, respectively. Specifically, the CL results indicate one of the causes of the 3.35-eV emission. An assumption that the emission is related to the square pits on the film is adopted. The origin of the pits needs further investigation in the future.

We extend our thanks for the electroscope support of the Public Center for Characterization and Test, Suzhou Institute of Nano-tech and Nanobionics, Chinese Academy of Sciences. This work was supported by the National Natural Science Foundation (Nos. 60990311 and 60676004) and the Key Basic Research Project of Shanghai Science and Technology (No. 10JC1415700).

References

1. T. Wang, X. Guo, Y. Fang, B. Liu, and G. Shen, Chin. Opt. Lett. **4,** 416 (2006).
2. S. M. Thahab, H. A. Hassan, and Z. Hassan, Chin. Opt. Lett. **7,** 226 (2009).
3. H. Liu, Q. Kan, C. Wang, F. Yu, X. Xu, and H. Chen, Chin. Opt. Lett. **7,** 918 (2009).
4. P. Waltereit, O. Brandt, A. Trampert, H. T. Grahn, J. Menniger, M. Ramsteiner, M. Reiche, and K. H. Ploog, Nature **406,** 865 (2000).
5. K. Xu, J. Xu, P. Deng, R. Qiu, and Z. Fang, Phys. Stat. Sol. (a) **176,** 589 (1999).
6. H. Maruska, D. Hill, M. Chou, J. Gallagher, and B. Chai, Opto-Electon. Rev. **11,** 7 (2003).
7. S. Ghosh, P. Waltereit, O. Brandt, H. T. Grahn, and K. H. Ploog, Phys. Rev. B **65,** 75202 (2002).
8. Y. J. Sun, O. Brandt, U. Jahn, T. Y. Liu, A. Trampert, and S. Cronenberg, J. Appl. Phys. **92,** 5714 (2002).
9. H. Lin, S. Zhou, H. Teng, T. Jia, X. Hou, S. Gu, S. Zhu, Z. Xie, P. Han, and R. Zhang, J. Alloy. Compd. **479,** L8 (2009).
10. J. Zou, S. Zhou, X. Zhang, F. Su, X. Li, and J. Xu, Chin. Opt. Lett. **3,** 494 (2005).
11. T. Jia, S. Zhou, H. Teng, H. Lin, X. Hou, Y. Li, W. Li, J. Wang, J. Liu, J. Huang, K. Huang, M. Zhang, J. Wang, and K. Xu, J. Crys. Growth **318,** 483 (2010).
12. P. P. Paskov, R. Schifano, T. Malinauskas, T. Paskova, J. P. Bergman, B. Monemar, S. Figge, D. Hommel, B. A. Haskell, P. T. Fini, J. S. Speck, and S. Nakamura. Phys. Status Solidi. C **3,** 1499 (2006).
13. F. Wu, M. D. Craven, S. H. Lim, and J. S. Speck, J. Appl. Phys. **94,** 1804 (2003).
14. M. A. Reshchikov and H. Morko, J. Appl. Phys. **97,** 061301 (2005).
15. C. Stampfl and C. G. Van de Walle, Phys. Rev. B **57,** 15052 (1998).